APPLIED GEOPHYSICS, Vol.20, No.2 (June 2023), P.186–197, 11 Figures.
DOI:10.1007/s11770-023-1052-9

Geostatistical inversion method based on seismic waveform similarity

Ni Xue-Bin[1], Zhang Jia-Jia[1*], Chen Kang[2], Zhang Guang-Zhi[1], Wang Bao-Li[1], Liu Zhuo-Fan[1], and Lin Ying[1]

Abstract: Seismic stochastic inversion method has received much attention because of its considerable advantage of having higher vertical resolution than deterministic inversions. However, due to the lack of cross-well data, the inversion results typically exhibit poor lateral continuity. Furthermore, the inversion efficiency is low, and the inversion result is highly random. Therefore, this study proposes a geostatistical seismic inversion method constrained by a seismic waveform. The correlation coefficient of seismic data is used to measure the similarity of the seismic waveforms, replacing the traditional variogram for sequential Gaussian simulation. Under the Bayesian framework, the Monte Carlo–Markov Chain (MCMC) algorithm is combined with the constraints of seismic data to randomly perturb and optimize the simulation results for obtaining the optimized parameter inversion results. The model data tests show that the initial model based on seismic waveform constraints can accurately describe the spatial structure of the subsurface reservoir. In addition, perturbing and optimizing initial model can increase the convergence speed of the Markov chain and effectively improve the accuracy of the inversion results. In this paper, the proposed geostatistical inversion method is applied to the actual seismic data of an oil field. Under the constraints of the stochastic simulation process and objective function, the geological information contained in the seismic waveforms is fully mined, and a theoretical foundation is provided for realizing the multidata joint-constrained seismic inversion.
Keywords: seismic waveform correlation coefficient, sequential Gaussian simulation, initial model, Monte Carlo–Markov Chain algorithm

Introduction

Seismic inversion has been widely used for the exploration and development of thin reservoirs of oil and gas to obtain the elastic parameters of subsurface media and describe the changes in the reservoir spatial structure. Limited by the seismic frequency band, deterministic seismic inversion cannot meet the requirements of high-resolution exploration. Logging data is used as conditional data for stochastic inversion to improve the vertical resolution of inversion results (Wang et al., 2018). However, such inversion results often encounter problems of strong randomness and low lateral continuity (Sams and Saussus, 2008, 2010; Yin et al., 2014). Hence, research on how to maximize

Manuscript received by the Editor March 21, 2023; revised manuscript received April 21, 2023.
1. School of Geosciences, China University of Petroleum (East China), Qingdao 266580, China
2. Research Institute of Exploration and Development, PetroChina Southwest Oil and Gas Field Company, Chengdu 610041, China
*Corresponding author: Zhang Jia-Jia (Email: zhangjj@upc.edu.cn).

the use of reservoir parameter information carried by seismic data has become an important direction for realizing high-resolution exploration. Taking seismic data and geostatistical characteristics as constraints and prior information, respectively, multiple reservoir parameter models can be built using geostatistical inversion methods to combine stochastic simulation with stochastic inversion (Durrani et al., 2021). Statistical analyses of these models can improve the prediction accuracy of their inversion results and further describe the thin reservoir structure characteristics in detail. Although stochastic inversion (Hass and Dubrule, 1994) was effectively utilized to improve the vertical resolution of inversion results using the strategy of channel-by-track simulation, the calculation efficiency of inversion results was not high. Therefore, simulated annealing (Debeye et al., 1996), Monte Carlo (Kane et al., 1999), and genetic algorithms (Azevedo et al., 2015) were successively introduced to randomly perturb simulated results for obtaining globally optimal inversion results.

To stimulate the three parameters of P-wave velocity, S-wave velocity, and density, Contreras et al. (2005) prestack seismic data need to be combined with geostatistical simulation, which enables the development of the stochastic inversion from post- to prestack, providing more information on the fine description of the subsurface structure and prediction of reservoir parameters. Escobar et al. (2006) proposed a fast prestack stochastic inversion method based on the sequence grid, greatly improving computational efficiency of stochastic inversion. Based on the spectrum simulation proposed by Francis (2006a, 2006b), Wang et al. (2015) adopted a fast Fourier transform moving average (FFT-MA) spectrum simulation algorithm to construct prior information in the frequency domain. When FFT-MA algorithm is combined with the gradual deformation method, the computational efficiency is improved. Yang and Mrinal (2016) combined a very fast simulated annealing algorithm with greedy annealed importance sampling to improve the inversion accuracy and increase the convergence speed.

Meanwhile, the application of seismic data has developed rapidly in recent years. For example, Pereira et al. (2019) built a more accurate prior model based on the lateral continuity of seismic data to make up for poor lateral continuity of logging data. The employment of seismic data as constraints can reduce the uncertainty in the solution space of the stochastic inversion (Dubrule et al., 1998; Wang and Zhao, 2010) and improve the accuracy of inversion results. Following the Bayesian framework, Buland and Omre (2003) applied prestack seismic data for constructing the likelihood function and obtained the three parameters of P- and S-wave velocities and density through direct inversion. Zhang et al. (2016) realized the classification of seismic waveforms and identification of seismic phases, while Song et al. (2019) proposed dynamic sub-windows matching as a new similarity measure to classify seismic waveforms. To obtain a subsurface lithofacies model and realize reservoir prediction, Abdel-Fattah et al. (2020) further excavated the information contained in seismic data and combined seismic attribute information with stochastic inversion results. Chen et al. (2020) proposed a seismic meme inversion method and analyzed the intrinsic relation between the seismic waveform and high-frequency logging information to realize the thin inter-reservoir prediction in continental basins. Zhou et al. (2021) established an initial model with waveform indications using the similarity of seismic waveforms. By using the Metropolis–Hastings (M–H) sampling algorithm, the initial model was perturbed multiple times randomly, following which the best inversion results were obtained. In addition, the seismic meme inversion method has been widely applied to actual work areas for achieving the accurate prediction of thin inter-reservoirs (Gao et al., 2017; Li et al., 2017; Wang et al., 2022; Chen et al., 2022). In this paper, a certain geophysical mapping relation between the low-frequency seismic waveform and high-frequency logging information is determined based on the correlation between logging curves and the seismic waveform in similar sedimentary environments. Additionally, a method has been proposed for using the lateral variation of seismic waveforms to guide high-frequency logging information, i.e., the correlation coefficient of seismic waveforms is used to guide the logging data modeling. Following the principles of the ordinary Kriging interpolation, we derived a sequential Gaussian simulation method based on the seismic waveform similarity. The initially constructed model with the seismic waveform indication can overcome the smoothness problem commonly found in the Kriging interpolation. Further, we used the MCMC algorithm to perturb and optimize the initial model and combined the results of the algorithm with seismic data constraints to effectively improve the lateral continuity of inversion results and enhance the accuracy and efficiency of stochastic inversion.

Theory and method

Mapping relationship between seismic waveform and reservoir parameters

Abundant geological information can be found in seismic waveforms, and its variation information, such as amplitude, phase, and frequency, indicates the characteristics of subsurface reservoirs (Hu et al., 2018). At present, the reflection wave is most commonly used in seismic inversion with a frequency range of 30–70 Hz. The frequency of seismic waves decreases gradually from the shallow layer to the middle and deep layers due to the absorption and attenuation of the formation, while the frequency of logging data can reach several kilohertz. As shown in Figure 1, the spectrum analysis of the single-trace seismic data reveals that its frequency is concentrated within 100 Hz, which is far smaller than the frequency range of the logging data. Therefore, the similarities of seismic waveforms can be used to guide the interpolation of logging curves. First, the mapping relationship between seismic waveform and the reservoir aspects that they characterize is defined, after which a suitable frequency range of the logging curves is selected to match the seismic and logging data.

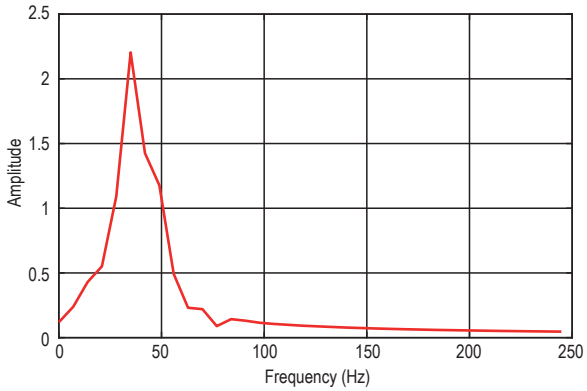

Figure 1. Spectrum of seismic records.

Simulating method of seismic waveform similarity based on SGS

The traditional seismic inversion method considers logging data as a known factor and reflects the spatial variation of inter-well reservoir parameters through variogram. Seismic data do not participate in guiding the construction of the initial model; hence, the information carried by the seismic waveform cannot be fully utilized.

An objective mapping relationship can be observed between the seismic records obtained in practice and the relevant parameters of the reservoir, based on which the seismic waveform similarity simulation can be conducted. Theoretically, seismic records can be expressed as the convolution of seismic wavelets and formation reflection coefficients. "Seismic inversion" refers to the inverse process of forward modeling and is the origin of the sequence of the formation reflection coefficients. The coefficient sequence can be obtained using the wave impedance information of a reservoir, after which the physical parameters of the subsurface medium can be solved. Figure 2 presents a schematic of the seismic forward and inversion process, which also reveals the objective relationship between the seismic waveform and reservoir physical property parameters. Therefore, using the similarities of seismic waveforms, the interpolation simulation of inter-well physical parameters is guided, which can then lead to the parameter model with better lateral continuity.

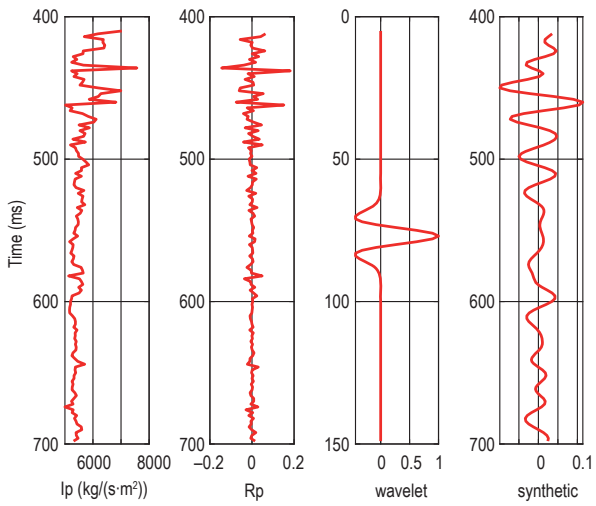

Figure 2. Schematic of seismic forward and inversion process.

Based on the convolution model, the lateral variation of seismic waveforms can reflect changes in reservoir parameters. Therefore, seismic waveform and high-frequency logging information can be used constructing initial models.

The key to realizing the seismic waveform similarity simulation is to complete the similarity optimization of seismic waveforms and determine the optimal sample and its corresponding weight coefficient. The algorithm for seismic meme indication inversion uses Kriging interpolation, which is based on the principle

of calculating the weight coefficient of some elastic or physical property parameter according to its partial measurement value for estimating the attribute value at a specific location. However, this method has a smoothing effect and is not suitable for reservoirs with severe lateral changes. To address this issue, we consider a sequential simulation algorithm for sampling random fields. The lateral variation of the seismic waveform is used to simulate the spatial inhomogeneity for efficiently realizing the reservoir parameters.

Figure 3 is a schematic of estimating the attribute value at a specific location using seismic waveform similarity simulation (Gao et al., 2017). Red represents the known positions, while purple represents the predicted positions. First, we compare the seismic waveform at the location to be predicted with all known locations. Subsequently, we obtain the seismic waveform correlation coefficient, in which the higher the seismic waveform correlation coefficient, the more similar the subsurface sedimentary characteristics at the two locations. Such sedimentary characteristics reflect the specific properties of reservoir parameters to a certain extent. Therefore, to complete the interpolation calculation of unknown reservoir parameters, the inherent relation between the seismic waveform and reservoir parameters can be used for guiding logging information. As shown in Figure 3, according to the seismic waveform correlation coefficient, the well samples at three locations are selected as known information and different weights are given to the well samples. This facilitates the calculation of the unknown parameters at the position to be predicted, in which there are two key steps:

1. Selecting the optimal well samples. First, we used a fixed time window to process the logging and seismic data and then establish the well and seismic data sample sets. Further, we calculated the correlation between the seismic waveform of the trace to be identified and that of the side trace of each well. Finally, we selected the well samples with high correlation as the effective statistical samples by ranking the correlation coefficients from high to low.

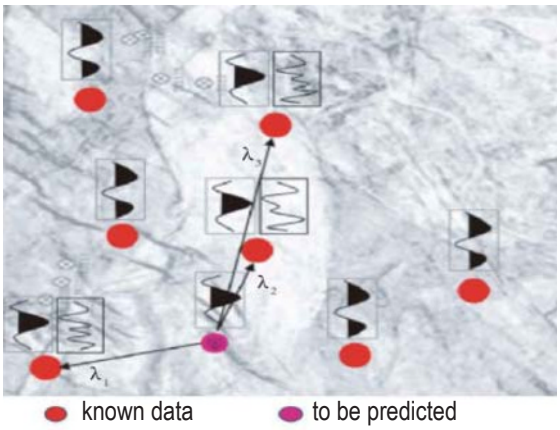

Figure 3. Schematic of similar simulation of seismic waveforms. (quoted from Gao, 2017).

2. Building the initial model. The selected well-sample curves are taken as known data to construct the initial model using sequential Gaussian simulation (SGS). The seismic waveform similarity coefficient is used instead of the variogram to describe the spatial structure changes in the reservoir. Therefore, the inversion results are more in line with the geological rules (Gao et al., 2017).

According to the comparison between the Kriging interpolation and SGS algorithm proposed by Zhao et al. (2010), after mathematical transformation, we find that the SGS value is equivalent to the sum of the Kriging interpolation result and a random deviation. Therefore, starting from the ordinary Kriging algorithm, we derive the formula for seismic waveform similarity simulation based on SGS. Here, we use the correlation coefficient of the seismic waveform instead of the variogram to complete the modeling of reservoir parameters.

The ordinary Kriging interpolation formula is as follows:

$$x_0^{ok} = \hat{\mu}_X + \sum_{i=1}^{n} \omega_i (x_i - \hat{\mu}_X) = \sum_{i=1}^{n} \omega_i x_i, \tag{1}$$

where x_0^{ok} is the data to be predicted; $\hat{\mu}_X$ is the mean value of the variable X, which is unknown; ω_i is the Kriging weight; and x_i is the known measurement value.

Given that Kriging interpolation satisfies unbiased estimation, it must satisfy the constraint that the sum of weights is 1:

$$\sum_{i=1}^{n} \omega_i = 1. \tag{2}$$

The expression for the estimated variance is as follows:

$$\begin{aligned} J &= \Delta(\hat{x}_0 - x_0) \\ &= \sum_{i=1}^{n}\sum_{j=0}^{n} \omega_i \omega_j Cov(x_i, x_j) - 2\sum_{i=1}^{n} \omega_i Cov(x_i, x_0) + \sigma^2 \\ &= \sum_{i=1}^{n}\sum_{j=0}^{n} \omega_i \omega_j \mathbf{C}_{ij} - 2\sum_{i=1}^{n} \omega_i \mathbf{C}_{i0} + \sigma^2, \end{aligned} \tag{3}$$

where $\mathbf{C}_{ij} = Cov(x_i, x_j)$ represents the covariance matrix of the two variables, and σ^2 is the variance within the region.

The formula for solving the similarity coefficient of the seismic waveform of two sets of data is as follows:

$$r_{ij} = \mathbf{C}_{ij} / (\sqrt{D(x_i)} \cdot \sqrt{D(x_j)}), \quad (4)$$

where r_{ij} represents the similarity coefficient of the seismic waveform at x_i and x_j, which is brought into Formula (3). Then, the variance is simplified as:

$$J = \sum_{i=1}^{n}\sum_{j=0}^{n} \omega_i \omega_j r_{ij} \sigma^2 - 2\sum_{i=1}^{n} \omega_i r_{ij} \sigma^2 + \sigma^2. \quad (5)$$

We use the similarity coefficient of the seismic waveform to obtain the weight coefficient, that is, to find the solution of x_j when the variance is the smallest, by combining this with the constraints of unbiased estimation. The objective function is constructed as follows:

$$W = J + 2\varphi(\sum_{i=1}^{n} \omega_i - 1), \quad (6)$$

where φ is the Lagrangian multiplier, and the objective function takes a derivative with respect to ω_i and φ, respectively. The matrix is constructed as follows:

$$\begin{bmatrix} r_{11} & r_{12} & \cdots & r_{1n} & 1 \\ r_{21} & r_{22} & \cdots & r_{2n} & 1 \\ \vdots & \vdots & \cdots & \vdots & \vdots \\ r_{n1} & r_{n2} & \cdots & r_{nn} & 1 \\ 1 & 1 & \cdots & 1 & 0 \end{bmatrix} \begin{bmatrix} \omega_1 \\ \omega_2 \\ \vdots \\ \omega_n \\ \varphi / \sigma^2 \end{bmatrix} = \begin{bmatrix} r_{10} \\ r_{20} \\ \vdots \\ r_{n0} \\ 1 \end{bmatrix}. \quad (7)$$

By solving the coefficient matrix, the weight coefficient based on the similarity coefficient of the seismic waveform can be obtained, which is inputted into Formula (1) to obtain the Kriging interpolation result. The addition of a random deviation to the interpolation result yields an implementation of SGS. This random deviation is the product of the standard deviation of the conditional distribution, in which the prediction should be made, and a random number that follows a standard normal distribution. This is expressed as:

$$x_0' = x_0^{ok} + l_m \sqrt{S(x_0)}, \quad (8)$$

where l_m is a random number that obeys the standard normal distribution, and $S(x_0)$ is the Kriging error variance, the formula for which is given by:

$$S(x_0) = \sigma^2 - \sum_{i=1}^{n} \omega_i C_{i0}. \quad (9)$$

The steps of the seismic waveform similarity simulation method based on SGS are as follows:

1. Set a random path and use the similarity coefficient of the seismic waveform to select well samples for each location to be predicted.

2. Use the similarity coefficient of the seismic waveform to calculate the weight coefficient of well samples at the position to be predicted and obtain the Kriging value and error variance.

3. To obtain the simulation value, add a random deviation based on the Kriging value.

4. Add the simulated value to a known sample set and combine it with the well sample at the next location to be predicted to obtain a new well-sample set.

5. Repeat Steps 2–4 according to the random path until the realization of SGS is obtained.

Markov chain–Monte Carlo (MCMC) algorithm

Based on the Bayesian framework, seismic inversion utilizes prior information and likelihood functions to obtain the posterior probabilities of inversion parameters. However, in actual seismic inversion, it is difficult to find the analytical solution of the posterior probability distribution. The MCMC inversion algorithm proposed in this paper is one such probabilistic inversion method. It has been widely used in seismic inversion due to its advantages, such as its ability to obtain the samples of the parameter posterior distribution through random sampling, avoid complicated calculations, and perform the uncertainty analysis of the inversion results (Sams et al., 1999; Hansen et al., 2006).

Furthermore, the MCMC algorithm connects the parameter distribution characteristics of the current moment with the previous moment by constructing a Markov chain. The model obtained using the similarity simulation of the seismic waveform is used as the initial distribution of parameters, and new parameter distribution characteristics are obtained through random perturbation and optimization. The convergence speed of the MCMC algorithm depends on the initial distribution, such that if the initial distribution is close to the distribution characteristics of the parameters, the Markov chain can quickly converge to a stable state. If the initial distribution is inaccurate, the inversion results may fall into a local minimum. Here, we use the simulation results obtained using seismic waveform similarity as the initial distribution of the MCMC optimization algorithm, which is more accurate than conventional low-frequency models. It is also beneficial for increasing the convergence speed of the Markov chain and avoiding local minima.

When constructing the Markov chain, it is assumed that the parameter distribution characteristics of the current moment are only related to the previous moment.

Therefore, the transition matrix can be simplified as:

$$\begin{aligned}&\mathbf{P}\left(X_t = s_j \middle| X_{t-1} = s_{j-1}, X_{t-2} = s_{j-2}, \ldots, X_0 = s_0\right)\\&= \mathbf{P}\left(X_t = s_j \middle| X_{t-1} = s_{j-1}\right),\end{aligned} \tag{10}$$

where $X(t)$ is regarded as a random variable, and s_j represents the parameter distribution characteristics of state j.

Here, we use $\mathbf{P}(t+1,t)$ to denote the transfer of the parameter distribution characteristics from $t+1$ to t, which is called the "proposal distribution". Therefore, the parameter distribution characteristic π_{t+1} at $t+1$ can be expressed by the proposal distribution and parameter distribution characteristics π_t at t as follows:

$$\pi_{t+1} = \mathbf{P}(t+1,t) \cdot \pi_t. \tag{11}$$

If the proposed distribution remains constant, the relationship between π_{t+1} and the initial distribution π_0 of the parameters can be established using the following recursion method:

$$\begin{aligned}\pi_{t+1} &= \pi_t \mathbf{P} = (\pi_{t-1}\mathbf{P})\mathbf{P}\\&= \pi_{t-1}\mathbf{P}^2\\&= \cdots\\&= \pi_0 \mathbf{P}^{t+1}.\end{aligned} \tag{12}$$

To avoid the inversion result falling into a local minimum, we use the acceptance probability formula to assess whether to transfer to a new parameter state. Let the acceptance probability formula $\alpha(0<\alpha<1)$ of transitioning from state θ to state υ be:

$$\alpha(\theta,\upsilon) = \min\left\{1, \pi_\upsilon \cdot \mathbf{P}(\upsilon,\theta) / (\pi_\theta \cdot \mathbf{P}(\theta,\upsilon))\right\}, \tag{13}$$

where π_θ and π_υ respectively indicate the parameter distribution characteristics of state θ and state υ, and $\mathbf{P}(\theta,\upsilon)$ and $\mathbf{P}(\upsilon,\theta)$ respectively indicate the proposal distribution from state θ to state υ and from state υ to state θ. Let us assume that a random number μ between 0 and 1 is generated and the size of μ and θ is compared. If $\mu < \alpha$, the new state υ is accepted; otherwise, the new state is not accepted. The reflection coefficient is calculated using reservoir parameters after perturbation, following which the synthetic seismogram is obtained. Further, the least square errors of the synthetic seismogram and observed seismogram are calculated as the objective function. The Markov chain is considered stable, and a dynamic representation of the posterior probability distribution can be realized when the maximum number of iterations is reached or if the objective function is less than the threshold value. Finally, multiple stochastic simulations are performed on the initial model with seismic waveform indications, and the posterior mean is taken as the optimal solution of the inversion result.

Model tests

Parameter settings

We selected a 2D impedance model for testing to verify the simulation theory of seismic waveform similarity. Aside from 80 traces of model data, the time range was 1150–1550 ms, and the data sampling interval was 1 ms. We extracted four traces of impedance data as pseudo-well data, segmented the data with a time window of 40 sampling points, and divided each trace of data into 10 samples. We used the impedance data to obtain the reflection coefficient and convolved it with the Ricker wavelet with a dominant frequency of 30 Hz to obtain synthetic data. Figure 4 shows the impedance model, the synthetic data with a signal-to-noise ratio of 2, and four traces of pseudo-well data.

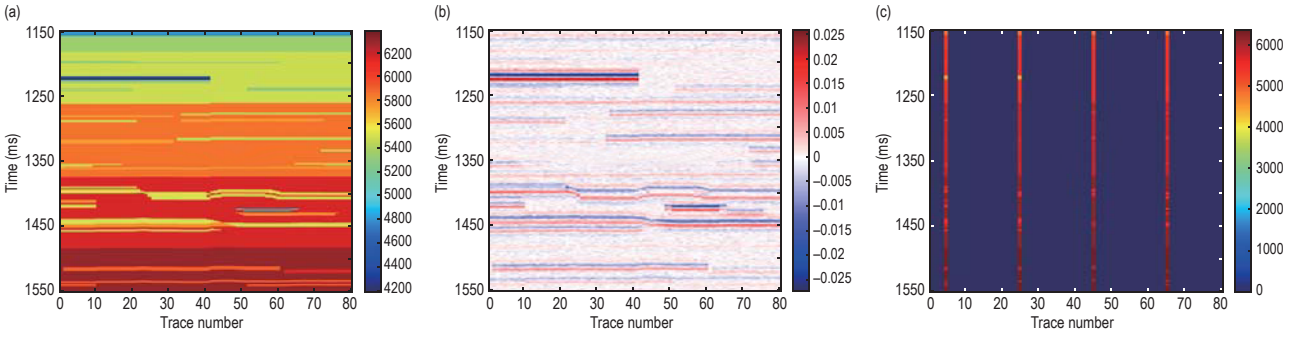

Figure 4. Impedance model data.
(a) Impedance model, (b) synthetic data with a signal-to-noise ratio of 2, and (c) four traces of pseudo-well data.

Simulation results

Based on the generated random path, we calculated the similarity coefficient of the seismic waveforms between the simulated and pseudo-well locations using Formula (4). Formula (7) is used to solve the weight coefficient, which is then incorporated into Formula (1) and Formula (8) to derive simulation results. Figure 5(a) presents the simulation results obtained using the inter-well interpolation based on the similarity of the seismic waveforms. The simulation results roughly reflect the basic shape of the impedance model, where a thin layer is relatively clear, and a low impedance feature at 1225 ms is obvious (marked by a black dashed oval in Figure 5(a). Figure 5(b) presents the comparison between the simulation result of the wave and real impedances of the 30th trace (marked by a black arrow in Figure 5(a)), where the waveform similarity coefficient of the wave impedance is 98.25%. This finding demonstrates that the simulation results can reflect the real model well when the lateral strata show minimal changes. Here, we use the simulation to obtain the initial model of the MCMC optimization algorithm, the initial model of the algorithm mitigates the low efficiency of stochastic inversion.

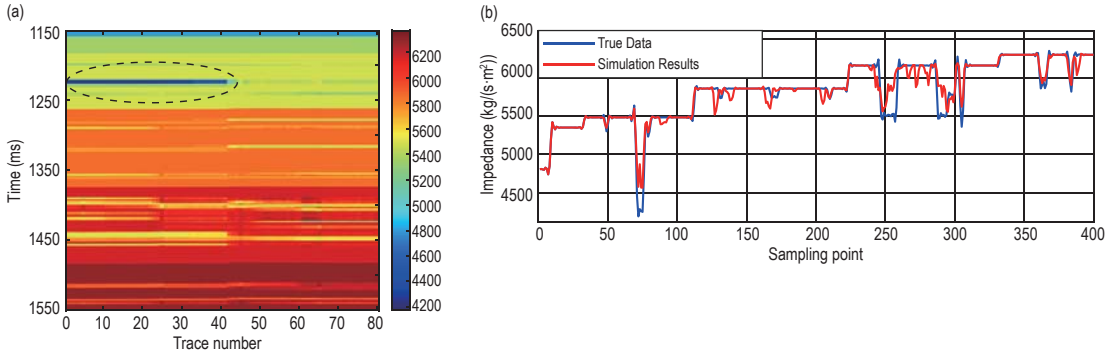

Figure 5. Simulated results. (a) Seismic waveform similarity simulation based on SGS and (b) comparison of the waveform similarity between the simulated and wave impedances at the well location (the 30th trace is selected).

Inversion results

We used the MCMC algorithm to perturb and update the results of the seismic waveform similarity simulation. The maximum number of iterations was set to 800. When the minimum square error of seismic records before and after the perturbation is less than 1e-6, the Markov chain is considered stable, and the final inversion result is obtained. Figure 6(a) presents the impedance inversion result. In 1350–1450 ms, thin layer inversion results are clear and lateral continuity is good (marked by a black dashed oval in Figure 6(a)). Figure 6(b) presents the comparison of the waveform similarity between the wave impedance inversion results of the 30th trace (marked by a black arrow in Figure 6(a)) and real wave impedance, where the waveform similarity coefficient reaches 99.14%. Compared with the wave impedance simulation results, the inversion results present a more accurate characterization of thin reservoirs (marked by a black dashed oval in Figure 6(b)). Figure 6(c) is the logarithmic error box plot of

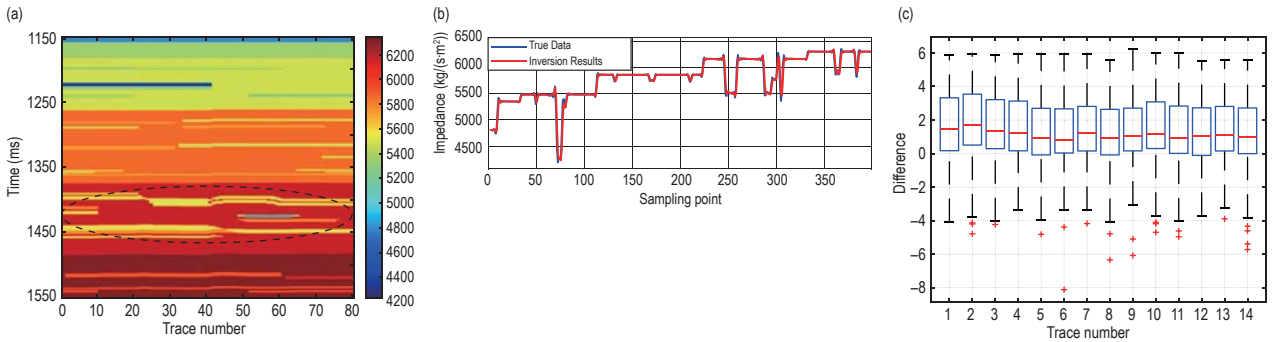

Figure 6. MCMC inversion result and error graph. (a) Impedance inversion result obtained using the MCMC algorithm, (b) comparison of the waveform similarity between the inverted wave impedance and wave impedance at the well location (the 30th trace is selected), and (c) logarithmic error box plot of the inversion result and impedance model.

the inversion result and impedance model. This plot indicates that the inversion results are highly consistent with the impedance model, and the error between the synthetic and the actual seismic record is very small. Furthermore, model testing reveals that the initial model based on the seismic waveform similarity simulation has a relatively high lateral resolution. Application of the MCMC algorithm can quickly stabilize the Markov chain and effectively improve the computational efficiency of the stochastic inversion and the accuracy of the inversion result. This method could also realize the full utilization of the seismic waveform. Therefore, by applying this method to the actual seismic data, we can obtain the inversion results with high lateral continuity and solve the problem of missing inter-well data.

Application of field data

Cut-off frequency test of the logging curves

The section of the work area is in a similar sedimentary environment. It has a total of 119 traces of seismic data with a time window range of 900–1100 ms and a sampling interval of 2 ms. Figure 7 shows the 2D section of the work area and two wells, A and B. We find that the frequency band of seismic data is typically within 100 Hz (Figure 1). However, the frequency band range of logging data can reach several thousand Hertz, making it difficult for us to realize the seismic waveform similarity simulation of actual seismic data. Therefore, we must filter the logging data to find the best cut-off frequency before applying the actual seismic data.

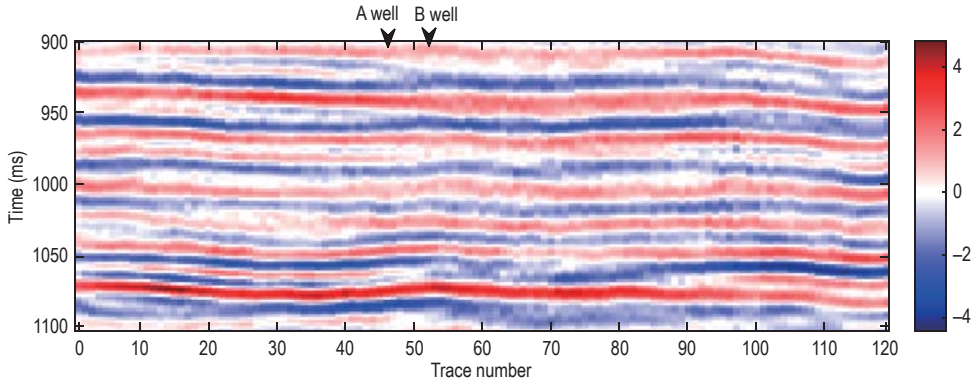

Figure 7. 2D seismic section of the work area

We extracted the near-wellbore seismic data from wells A and B and conducted Pearson linear correlation analysis on their waveform. Pearson's formula is as follows:

$$r_{XY} = \mathrm{cov}(X, Y) / (\sigma_X \sigma_Y), \quad (14)$$

where r_{XY} represents the strength of the linear relationship between variable X and variable Y, and the value range is [−1,1]. When it is greater than 0, the value indicates that the two variables are positively correlated; furthermore, the greater r is, the stronger the linear relationship is. In addition, cov(X, Y) represents the covariance of the two variables, and σ_X and σ_Y represent the standard deviations of the two variables, respectively. Through calculation, the waveform similarity coefficient of seismic data reaches 76.3%, as shown in Figure 8. This result indicates that the seismic waveform has a positive linear correlation in a similar sedimentary environment. Thus, the intrinsic relationship between the seismic waveform characteristics and the subsurface sedimentary characteristics is proven from the side.

We performed the same linear correlation analysis on the waveform of the wave impedance of the two wells, as shown in Figure 9(a). The results show that the waveform similarity coefficient is 68.61%, which is much lower than the waveform similarity coefficient

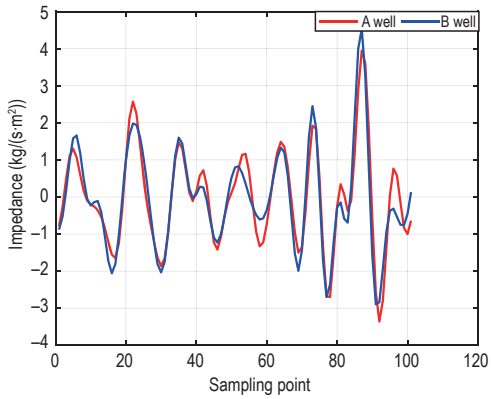

Figure 8. Comparison of seismic waveform similarities at two wells.

of the seismic data. This is because the logging curves are full-band, high-frequency components that tend to reduce their correlation coefficient. Due to the need to filter the logging curves to improve the waveform similarity coefficient of the wave impedance of the two wells, we selected filters with cut-off frequencies of 500, 400, 300, 200, and 100 Hz to filter the logging curves. The waveform similarities of the wave impedance are calculated as shown in Figure 9 (b–f), which include 71.19%, 71.52%, 72.13%, 74.05% and 77.79%, respectively.

Figure 9 shows that high-frequency components in the logging curves are filtered out as the cut-off frequency decreases step by step. The correlation coefficients of

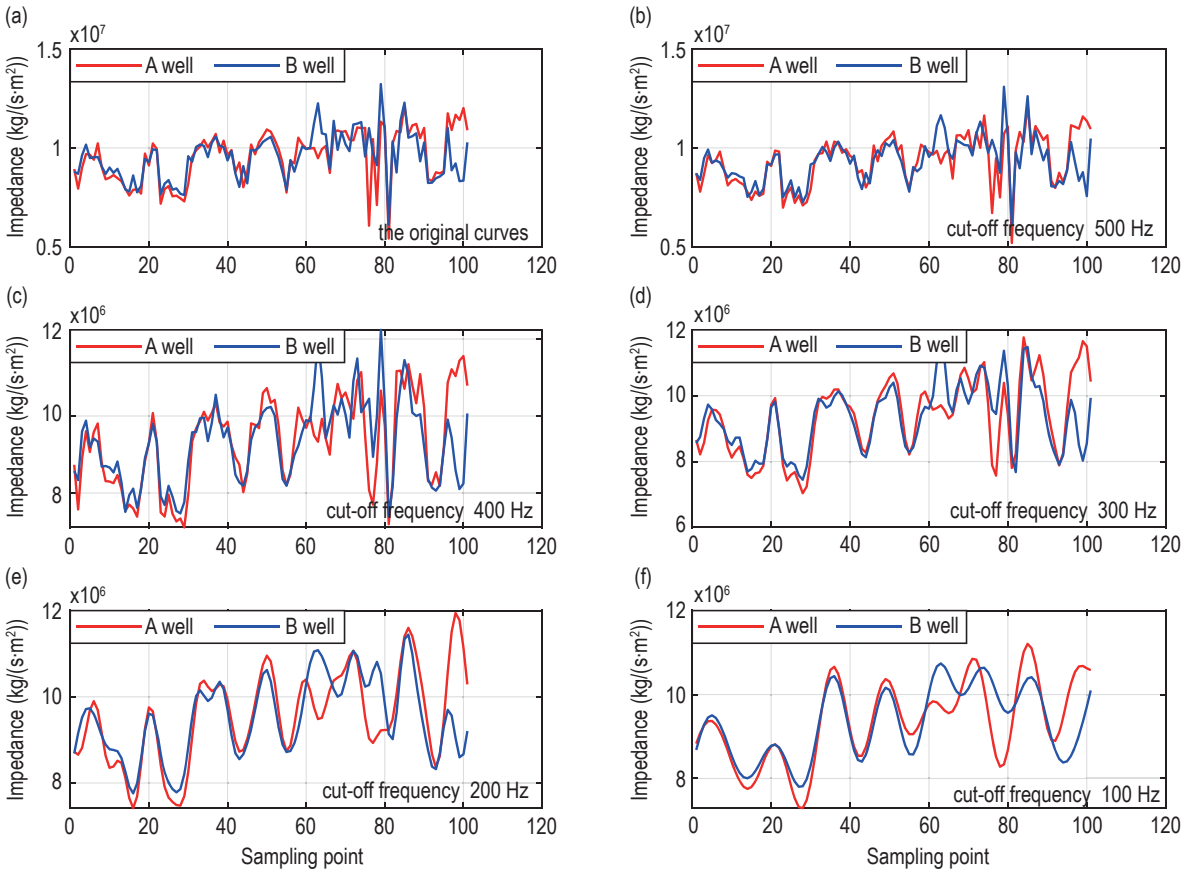

Figure 9. Comparison of the waveform similarities of the wave impedances of two wells at different cut-off frequencies.

the P-wave impedance curves increase continuously, which tends to be consistent with the seismic waveform similarity. Therefore, before using seismic waveform similarity simulation, filtering of logging curves is necessary for determining the best cut-off frequency. When the cut-off frequency is 100 Hz, the correlation coefficient of the P-wave impedance curves of the two wells is close to the seismic waveform similarity. Therefore, we can establish the relation between the seismic waveform and high-frequency logging information. Seismic waveform characteristics can reflect subsurface sedimentary characteristics and then indicate changes in reservoir parameters. Furthermore, an initial model reflecting the subsurface spatial structure and reservoir parameter changes can be obtained by guiding the interpolation simulation of the P-wave impedance curves with seismic waveform.

Simulation results

We simulated and inverted the 2D seismic section in figure 7 after determining the optimal cut-off frequency of logging curves. Additionally, we calculated the seismic waveform similarity coefficient between the location to be simulated and the well location, thereby solving the weight coefficients of different wells. Further, we integrated this into Formula (1) and Formula (8) to obtain simulation results. Figure 10(a) shows that good results of the lateral continuity of the seismic waveform similarity simulation are obtained, verifying the feasibility of the simulation method in the actual

working area. Figure 10(b) presents the comparison between the simulated wave impedance and on well locations at the thirteenth trace and the thirty-ninth trace, where the correlation coefficients reach 87.08% and 88.96%, respectively. Furthermore, the results obtained from the seismic waveform similarity simulation based on SGS have high reliability, can be used as the initial model of the MCMC algorithm to facilitate rapid convergence of the impedances to a stable state.

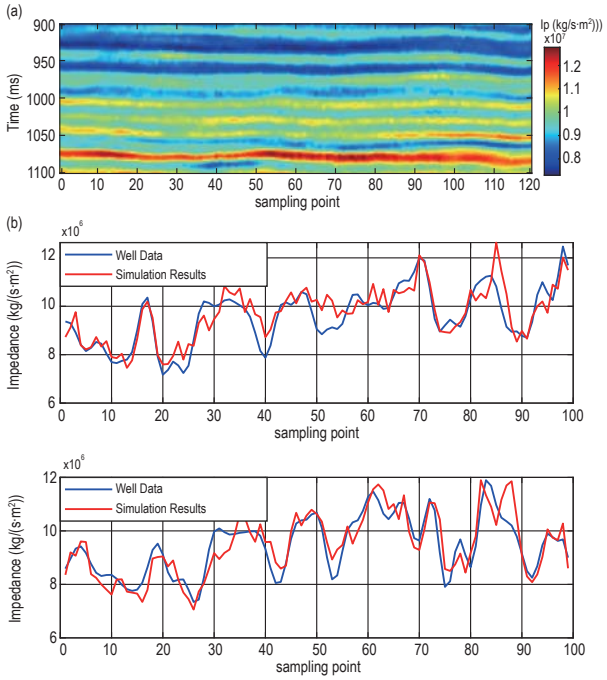

Figure 10. Seismic waveform similarity simulation based on SGS. (a) Wave impedance simulation results and (b) comparison of the wave impedance at the well location and simulated wave impedance.

Inversion results

The simulation results are considered as the initial model, which was perturbed by the MCMC algorithm. We set the maximum number of iterations to 800 and the threshold to 1e-6. When the minimum square errors of the seismic records before and after the perturbation are less than this threshold value, the Markov chain is considered stable, as shown in the inversion results in Figure 11(a). Figure 11(b) shows the similarity between the inverted wave impedances and wave impedances on well locations at the thirteenth trace and the thirty-ninth trace, with similarity coefficients of 93.05% and 94.04%, respectively. The statistical histogram of inversion results and wave impedance logging curves in Figure 11(c) reveals that the inversion results are consistent with the distribution of the wave impedance logging curves. These findings indicate that the spatial structure and trend of the inversion results are consistent with the lateral variation of the seismic waveform. These inversion results are in line with the subsurface sedimentary characteristics and the prior information of logging curves. A comparison of the inversion results with the simulation results reveals that the inversion results of thin layers are clearer at 1050–1100 ms. The inversion results are also consistent with the histogram distribution law of the well data, proving the feasibility of the stochastic inversion method based on the seismic waveform similarity.

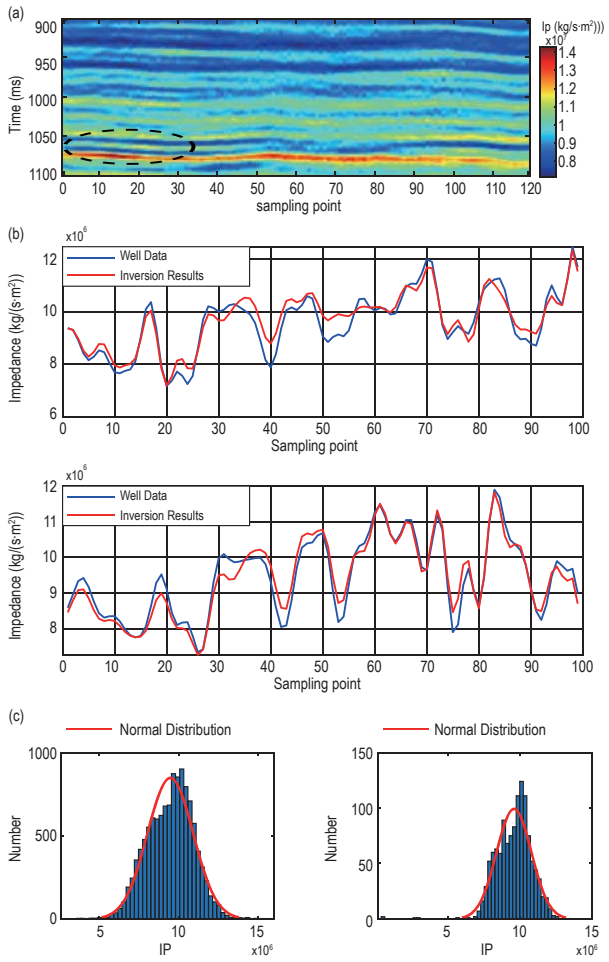

Figure 11. Wave impedance inversion results based on the seismic waveform similarity simulation. (a) Wave impedance inversion results, (b) comparison of wave impedance at the well location and inverted wave impedance, and (c) statistical histogram comparison of inversion results (left) and well data (right).

Conclusions

A geostatistical inversion method based on the seismic

waveform constraints is proposed in this paper to solve the problem of poor lateral continuity of inversion results due to a lack of inter-well data. First, we used the convolution model to demonstrate the internal relation between the seismic waveform and reservoir parameters, reflecting the spatial structure of subsurface media. Subsequently, we analyzed the best cut-off frequency of logging curves, following which a new method for calculating the weight coefficient of the seismic waveform was proposed. We used the lateral variation of the seismic waveform to drive high-frequency logging information and subsequently establish an initial model with waveform indication, which describes the spatial distribution of the underground reservoir more accurately.

Under the Bayesian framework, we used the MCMC stochastic inversion method to construct the posterior probability distribution function of the co-constraint of the seismic waveform and logging curve. Further, we introduced the M–H sampling algorithm to randomly simulate the initial model parameters multiple times and then the posterior mean is used as the optimal solution of the model parameters. This method effectively improves the computation speed of the inversion method and the lateral continuity of inversion results while also realizing high-resolution inversion. Additionally, the model and actual data inversion results demonstrate that the seismic waveform similarity simulation based on SGS can effectively overcome the smoothness of the Kriging interpolation and improve the lateral continuity of simulation results. Finally, the initial model with waveform indication can make the Markov chain converge quickly. Meanwhile, the accuracy of the stochastic inversion is improved.

Acknowledgments

This work was kindly supported by the National Natural Science Foundation of China [Grant Nos. 42174146; 42074136;42174144], and Innovation Fund Project for Graduate Students of China University of Petroleum (East China) [Grant No. 23CX04015A]. Thanks to Geosoftware for software support. The authors would like to thank the editors and anonymous reviewers for their valuable comments.

References

Abdel-Fattah, M. I., Pigott, J. D., and El-Sadek, M. S., 2020, Integrated seismic attributes and stochastic inversion for reservoir characterization: insights from Wadi field (NE Abu-Gharadig Basin, Egypt): Journal of African Earth Sciences, 161, 103661.1–103661.14.

Azevedo, L., Nunes, R., Soares, A., et al., 2015, Geostatistical seismic AVO inversion directly for facies-real case application: 77th Annual international Meeting, EAGE, Expanded Abstracts, 1–5.

Buland, A., and Omre, H., 2003, Bayesian linearized AVO inversion: Geophysics, **68**(1), 185–198.

Chen, X., Zhao, M., Cui, J. B., et al., 2022, Seismic Motion Inversion Based on Geological Conditioning and Its Application in Thin Reservoir Prediction, Middle East: Annual international Meeting, SPE, Expanded Abstracts, 211631.

Chen, Y. H., Bi, J. J., Qiu, X. B., et al., 2020, A method of seismic meme inversion and its application: Petroleum Exploration and Development, **47**(6), 1235–1245.

Contreras, A., Torres-Verdin, C., Kvien, K., et al., 2005, AVA stochastic inversion of pre-stack seismic data and well logs for 3D reservoir modeling: 67th Annual international Meeting, EAGE, Expanded Abstracts, cp–1–00310.

Debeye, H., Sabbah, E., and Van der Made, P. M., 1996, Stochastic inversion: EAGE Winter Symposium-Reservoir Geophysics, the Road Ahead, European Association of Geoscientists & Engineers, p 22–98.

Dubrule, O., Thibaut, M., Lamy, P., et al., 1998, Geostatistical reservoir characterization constrained by 3D seismic data: Petroleum Geoscience, **4**(2), 121–128.

Durrani, M. ZA., Talib, M., Ali, A., et al., 2021, Characterization of carbonate reservoir using post-stack global geostatistical acoustic inversion approach: A case study from a mature gas field, onshore Pakistan: Journal of Applied Geophysics, **188**(1), 104313.

Escobar, I., Williamson, P., Cherrett, A., et al., 2006, Fast geostatistical stochastic inversion in a stratigraphic grid: 76th Annual international Meeting, SEG, Expanded Abstracts, 2067–2071.

Francis, A. M., 2006, Understanding stochastic inversion: Part 1: First Break, **24**(11), 69–77.

Francis, A. M., 2006, Understanding stochastic inversion: part 2: First Break, **24**(12), 79–84.

Gao, J., Bi, J. J., Zhao, H. S., et al., 2017, Seismic waveform inversion technology and application of thinner reservoir prediction: Progress in Geophysics, **32**(1), 142–145.

Haas, A., and Dubrule, O., 1994, Geostatistical inversion-a sequential method of stochastic reservoir modelling constrained by seismic data: First break, **12**(11), 561–569.

Hansen, T. M., Journel, A. G., Tarantola, A., et al., 2006, Linear inverse Gaussian theory and geostatistics: Geophysics, **71**(6), R101–R111.

Hu, W., Qi, P., Yang, J. F., et al., 2018, Application of seismic motion inversion in identification of tight thin super deep reservoirs: Progress in Geophysics, **33**(2), 620–624.

Kane, J., Rodi, W., Herrmann, F., et al., 1999, Geostatistical seismic inversion using well log constraints: 69th Annual international Meeting, SEG, Expanded Abstracts, 1504–1507.

Li, B. J., Bi, J. J., Wei, S. D., et al., 2017, Application of waveform inversion technique in prediction of beach bar sandstone reservoir: 87th Annual international Meeting, SEG, Expanded Abstracts, 686–689.

Pereira, P., Azevedo, L., Nunes, R., et al., 2019, The impact of a priori elastic models into iterative geostatistical seismic inversion: Journal of Applied Geophysics, **170**, 103850–103850.

Sams, M., and Saussus, D., 2008, Comparison of uncertainty estimates from deterministic and geostatistical inversion:78th Annual international Meeting, SEG, Expanded Abstracts, 1486–1490.

Sams, M., and Saussus, D, 2010, Comparison of lithology and net pay uncertainty between deterministic and geostatistical inversion workflows: First break, **28**(2), 35–44.

Sams, M. S., Atkins, D., Said, N., et al., 1999, Stochastic inversion for high resolution reservoir characterisation in the Central Sumatra Basin: Annual international Meeting, SPE, Expanded Abstracts, 57260–57260.

Song, C. Y., Liu, Z. N., She, B., et al., 2019, Seismic waveform classification via a new similarity measure: 89th Annual international Meeting, SEG, Expanded Abstracts, 2438–2442.

Wang, B. L., Yin, X. Y., Ding, L. X., et al., 2015, Study of fast stochastic inversion based on FFT-MA spectrum simulation: Chinese Journal of Geophysics, **58**(2), 664–673.

Wang, J. B., Li, Z. J., Chen, C., et al., 2022, Predicting gas content in coalbed methane reservoirs using seismic waveform indication inversion: a case study from the Upper Carboniferous Benxi Formation, eastern Ordos Basin, China: Acta Geophys, **70**(2), 623–638.

Wang, J. H., and Zhao, W., 2010, Research on geostatistical modeling method constrained by seismic data: Offshore Oil (in chinese) **30**(4), 46–49.

Wang, X. D., Yin, X. Y., Jin, H., et al., 2018, Pre-stack seismic stochastic inversion and application on real data: Progress in Geophysics, **33**(6), 2471–2476.

Yang, X., and Mrinal K, S., 2016, Stochastic seismic inversion using greedy annealed importance sampling: Journal of Geophysics and Engineering, **13**(5), 786–804.

Yin, X. Y., Sun, R. Y., Wang, B. L., et al., 2014, Simultaneous inversion of petrophysical parameters based on geostatistical a priori information: Applied Geophysics, **11**(3), 311–320.

Zhang, S. H., Xu, Y., and Abu-Ali, M., 2016, Characterizing stratigraphic traps using improved waveform classification seismic facies analysis: an example from central Saudi Arabia: First Break **34**(12), 77–84.

Zhao, Y. F., Sun, Z. Y., and Chen, J., 2010, Analysis and comparison in arithmetic for Kriging interpolation and sequential Gaussian conditional simulation: Journal of Geo-Information Science, **12**(6), 767–776.

Zhou, S. S., Yin, X. Y., and Pei, S., 2021, Monte Carlo-Markov Chain stochastic inversion constrained by seismic waveform: Oil Geophysical Prospecting, **56**(3), 543–554+592+413.

Ni Xue-Bin, a master's student, is currently studying at the School of Earth Science and Technology, China University of Petroleum (East China). Her main interests are reservoir geophysics, seismic data processing and interpretation methods, and prestack reservoir prediction. Unit: School of Earth Science and Technology, China University of Petroleum (East China); Postcode: 266580; Tel: 17806281886; E-mail: Z21010085@s.upc.edu.cn

Zhang Jia-Jia is an associate professor at the China University of Petroleum (East China). He graduated from the Ocean University of China in 2007 with a bachelor's degree in Earth Information Science and Technology, with a master's degree in Earth Exploration and Information Technology from the Ocean University of China in 2010, and in 2013 with a doctorate degree in Earth Exploration and Information Technology from China Petroleum Exploration and Development Research Institute. His main research interests include seismic rock physics and prestack reservoir prediction. Unit: School of Earth Science and Technology, China University of Petroleum (East China); Postcode: 266580; Tel: 15205326882; E-mail: zhangjj@upc.edu.cn